Linear-quadratic-Gaussian control for adaptive optics systems using a hybrid model

Douglas P. Looze

Department of Electrical and Computer Engineering, University of Massachusetts, Amherst, Massachusetts 01003, USA (looze@ecs.umass.edu)

Received April 14, 2008; revised August 28, 2008; accepted October 14, 2008; posted October 28, 2008 (Doc. ID 94916); published December 3, 2008

This paper presents a linear-quadratic-Gaussian (LQG) design based on the equivalent discrete-time model of an adaptive optics (AO) system. The design model incorporates deformable mirror dynamics, an asynchronous wavefront sensor and zero-order hold operation, and a continuous-time model of the incident wavefront. Using the structure of the discrete-time model, the dimensions of the Riccati equations to be solved are reduced. The LQG controller is shown to improve AO system performance under several conditions. © 2008 Optical Society of America

OCIS codes: 010.1080, 010.1285.

1. INTRODUCTION

The objective of an adaptive optics (AO) system in astronomy is to reduce the aberrations introduced by the Earth's atmosphere to the wavefront from an observed object [1,2]. The design of an AO system must account for many sources of error. As is usual, this paper will assume that these errors are independent and can be considered separately (c.f. [1]). This paper will address the problem of designing the feedback compensation to minimize the temporal errors in the AO system. The feedback system will be designed based on optimization using dynamic models of the AO system components. The feedback system is a linear-quadratic-Gaussian (LQG) controller based on a discrete-time model of the AO system presented by [3].

Optimization has been used often in the design of AO controllers. Gendron and Léna [4] optimized integrator gains of a modal controller based on the signal-to-noise ratio of the modes. Ellerbroek *et al.* [5] simultaneously optimized the modal basis and integrator gains (control bandwidths). Dessenne *et al.* [6] optimized the parameters of a predictive controller using measurements of the incident wavefront (IWF). The Taylor hypothesis and a layer model of the atmosphere (c.f. [1]) have been exploited by Poyneer and Véran [7] to estimate the IWF with a Kalman filter and apply the estimate to the deformable mirror (DM).

LQG techniques (and equivalents) were first applied to AO systems by Paschall and Anderson [8] with a controller design based on a system that modeled the first 14 Zernike modes (ignoring the piston mode) with spectra generated by first-order, independent Markov models. Looze *et al.* [9] designed an LQG modal controller based on a model of the spatial modes and the measured modal spectra of the IWF. Le Roux *et al.* [10] developed and simulated LQG designs for both classical and multiconjugate AO (MCAO) systems. An LQG design of a static controller was presented by Wiberg *et al.* [11]. Looze [12] analyzed the structure of an LQG controller with the assumption that the intraframe response of the residual was not significant. Reference [12] also showed that the standard integral AO controller is an LQG controller when the loop delay and DM dynamics are neglected. The efficiency of an LQG controller was first demonstrated in a laboratory experiment for both classical AO and MCAO systems by Petit *et al.* [13,14]. The classical AO experiment illustrated the ability of an LQG controller to reject vibrations. Hinnen *et al.* [15] used measurement data to specify the H_2 (LQG) parameters of an AO controller and demonstrated performance improvement in a laboratory experiment. The structure of an LQG controller and its relation to integral controllers was investigated by Kulcsár *et al.* in [16].

All these control design techniques (referred to as LQG, Kalman based, or H_2) are equivalent. Each controller embeds a Kalman filter in its design. The LQG and H_2 techniques use different underlying mathematical models of the disturbance process. The LQG optimization models the incident turbulence and measurement noise as Gaussian processes, the system [DM and wavefront sensor (WFS)] as linear, and the objective as quadratic (a linear combination of covariances); H_2 optimization models the turbulence and measurement noise as deterministic and unknown except for their (weighted) H_2 norm. The objective is also given in terms of a (deterministic) H_2 norm of a performance signal. Although the controllers given by these two designs are identical, the stochastic interpretation of signals by the LQG formulation is more natural to an AO system.

The individual control designs differ by using different underlying models of the AO system components. Many of the LQG designs assume a discrete-time model for the DM or IWF. Kulcsár *et al.* [16] showed that the frame-averaged residual was an equivalent statistic for the continuous-time residual variance when the control was applied at the beginning of a frame and the DM has no

temporal dynamics. The frame-averaged residual was then modeled in discrete time.

Each LQG design is "optimal" for the model for which it is designed. However, the feedback loop in an AO system involves both discrete-time and continuous-time signals. In particular, the DM surface, IWF, and residual wavefront are continuous-time signals. Designs based on discrete-time models [8–12] will generally not be optimal for the hybrid AO system because the design model differs from the equivalent discrete-time model of the AO system.

Both [3,16] show that the residual wavefront variance is the sum of the residual variance of the closed-loop discrete-time system and a term that is not affected by the controls. Consequently, the residual wavefront variance can be minimized using the equivalent discrete-time model of the hybrid AO system.

The hybrid LQG controller that is presented in this paper follows directly from the equivalent discrete-time model in [3]. The controller can incorporate both DM and IWF temporal dynamics. The hybrid LQG design does not assume that the beginning of the frame of the WFS is synchronized with the application of the DM commands via the zero-order hold (ZOH). The incorporation of DM dynamics, asynchronous WFS and ZOH, and a continuous-time model of the IWF are all developments beyond [16].

As is standard, the solution of the hybrid LQG control problem incorporates the separation principle [17] and is given in terms of the solution of two, discrete-time algebraic Riccati equations (AREs). The dimensions of AREs that must be solved are reduced using the structure of the hybrid discrete-time system.

The performance of the hybrid LQG controller is compared with the performances of LQG controllers based on a discrete-time approximation of an AO system ([10–15]), gain-optimized integral controllers, and the synchronous controller in [16]. It is shown that the use of the discrete-time approximation can result in poor performance for loop delays whose modulus is near a half-sample. In such cases, use of the hybrid discrete-time model of the AO system is essential.

2. ADAPTIVE OPTICS SYSTEM MODEL

A. Signal and Component Definitions and Models

A standard, single-conjugate AO system (with co-located guidestar and science object) is shown in Fig. 1. The incident light (wavefront ϕ^{tur}) is reflected from a DM with surface position s_m to form a residual wavefront ϕ^{res}. The feedback measurement signal is formed by measuring an approximation to the gradient (or curvature) of this residual using a WFS. The WFS forms its output by integrating the residual wavefront over the frame of a CCD camera and sampling the result at the end of the frame. The sampled signal is corrupted by additive noise $\tilde{\theta}$ to form a discrete-time measurement $\tilde{y}$. The outputs of the AO controller are discrete-time voltage commands $\tilde{a}$. These are converted by a ZOH into continuous-time voltages a to be applied to the DM. Thus, the measurement and control signals are inherently discrete time, while the residual wavefront (whose variance is the performance of the AO system) is a continuous-time signal. The structure of the feedback loop is a standard hybrid (sampled-data) system.

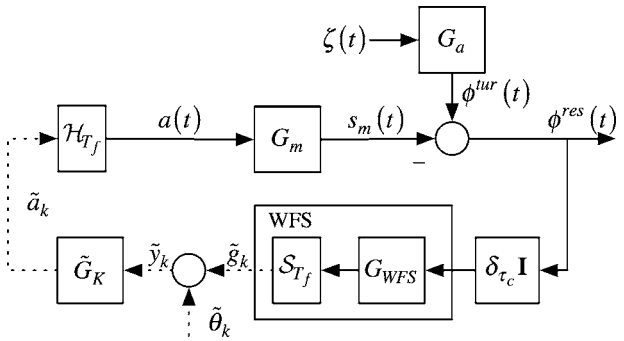

Fig. 1. Model of a classic AO system. Continuous-time signals (solid line) in the feedback loop are the incident phase ϕ^{tur}, the mirror surface s_m, the residual phase ϕ^{res}, and the actuator inputs a. Discrete-time signals (dashed line, tilde over signal name) include the measurement $\tilde{y}$, the measurement noise $\tilde{\theta}$, and the commanded actuator inputs $\tilde{a}$.

Since the discrete-time control $\tilde{a}_k$ is applied to the ZOH as soon as it is available, the sample time and the hold time are not physically simultaneous (c.f. [18–20]). All components of the computational delay (equal to τ_c for all signals and represented by the linear, time-invariant (LTI) operator δ_{τ_c}) will be regarded as occurring immediately prior to the WFS.

The output of the DM $s_m(t)$ can be either a vector of the mirror surface positions at points in the pupil (often, but not necessarily, at the actuator locations) or a vector of coefficients of a spatial modal decomposition of the mirror surface. In either case, it is assumed that the piston mode has been removed and that all other modes are stable. The IWF $\phi^{tur}(t)$ is represented using the same convention as the DM surface. The difference between these two vectors is the residual wavefront $\phi^{res}(t)$ and is supplied to both the science instrument and (with delay) to the WFS.

The DM and IWF are modeled in continuous time (see [3] for details) by stable, finite-dimensional, LTI systems:

$$\dot{x}_m(t) = A_m x_m(t) + B_m a(t), \qquad x_m(t) \in \mathbb{R}^{n_m}, \qquad a(t) \in \mathbb{R}^{m_m},$$

$$s_m(t) = C_m x_m(t) + D_m a(t), \qquad s_m(t) \in \mathbb{R}^{q}, \tag{1}$$

$$\dot{x}_a(t) = A_a x_a(t) + B_a \zeta(t), \qquad x_a(t) \in \mathbb{R}^{n_a}, \qquad \zeta(t) \in \mathbb{R}^{m_a},$$

$$\phi^{tur}(t) = C_a x_a(t), \qquad \phi^{tur}(t) \in \mathbb{R}^{q}, \tag{2}$$

$$\phi^{res}(t) = \phi^{tur}(t) - s_m(t) \in \mathbb{R}^{q}, \tag{3}$$

where $\zeta(t)$ is an uncorrelated, zero-mean, white-noise process with spectral unity and spectral density. Since the residual wavefront is sent to the science instrument, $\phi^{res}(t)$ is also the performance signal (whose steady-state aperture variance is the system performance).

The output of the WFS is inherently a discrete-time signal $\tilde{y}_k$ that is a linear function of the integral of the residual over a portion of one frame of the CCD camera. In this paper, it will be assumed that the integration interval used for the WFS measurement is the entire frame.

The linear function of the frame-integrated residual that defines the measurement is represented by multiplication by the geometry matrix H.

The computational loop delay τ_c includes the readout time of the CCD, the time needed to compute the gradients from the CCD readout, and the time needed to compute the control. Since the control is applied immediately, it also includes the asynchronous operation of the WFS and ZOH. The computational delay is represented by a diagonal, LTI operator as in Fig. 1.

The measurements produced by the WFS are corrupted by an additive zero-mean, white-noise sequence measurement noise $\tilde{\theta}_k \in \mathbb{R}^p$ with covariance $\Theta \in \mathbb{R}^{p\times p}$. Define

$$\tilde{\theta}_k \triangleq D_\theta \tilde{\theta}_{nk}, \qquad D_\theta = \sqrt{\Theta} \in \mathbb{R}^{p\times p}. \tag{4}$$

The WFS measurement is ($\mathcal{S}_{T_f}$ in Fig. 1 denotes the sample operator with sample period T_f):

$$\tilde{y}_k = g(kT_f) + \tilde{\theta}_k, \qquad g(t) = \frac{1}{T_f} H \int_{t-T_f-\tau_c}^{t-\tau_c} \phi^{res}(\sigma)\mathrm{d}\sigma. \tag{5}$$

The controller $\tilde{G}_K$ is also a finite-dimensional, LTI system:

$$\tilde{x}_{k+1} = A_K \tilde{x}_k + B_K \tilde{y}_k, \qquad \tilde{x}_k \in \mathbb{R}^{n_K},$$

$$\tilde{a}_k = C_K \tilde{x}_k + D_K \tilde{y}_k, \qquad \tilde{a}_k \in \mathbb{R}^m. \tag{6}$$

The actuator commands a are the output of a ZOH ($\mathcal{H}_{T_f}$ in Fig. 1):

$$a(t) = \tilde{a}_k \quad \text{for} \quad kT_f \leqslant t < (k+1)T_f. \tag{7}$$

A common measure of the quality of an image produced by a science instrument (and hence of AO system performance) is the Strehl ratio [1,2]. Assuming the extended Maréchal approximation is valid, the Strehl ratio is a strictly decreasing function of the residual (error) wavefront variance.

The temporal average of the residual wavefront variance is

$$V = \lim_{W\to\infty} \frac{1}{W} \int_0^W \mathcal{E}\{\phi^{res}(\sigma)^T \phi^{res}(\sigma)\}\mathrm{d}\sigma$$

$$= \lim_{W\to\infty} \frac{1}{W} \int_0^W \mathrm{tr}[P_{res}(\sigma)]\mathrm{d}\sigma, \tag{8}$$

where $P_{res}(t) \in \mathbb{R}^{m\times m}$ is the residual covariance matrix and tr(·) denotes the (matrix) trace of its argument. The expected value of the quadratic form in the integrand represents the residual variance at a point in time. This variance approximates the spatial integration of the residual if the components of the residual vector are values at points in the pupil. If the components of the residual vector are modal coefficients, the variance is the sum of squares of the coefficients. If necessary, additional weighting of the quadratic integrand in Eq. (8) can be incorporated to improve the accuracy of the quadratic form.

B. Discretization of the Adaptive Optics Model

The performance of the sampled-data AO model can be computed from the performance of a corresponding discrete-time model [3]. Throughout this section, it will be assumed that the computational loop delay is positive and no greater than one frame ($0 < \tau \leqslant T_f$). The discrete-time model can be readily modified to include zero delay or delays longer than one frame [3].

The discrete-time model that corresponds to the AO system is (see [3] for the details of the analytical forms and computations of the nonzero blocks of the discrete-time model)

$$\tilde{\mathbf{x}}_{k+1} = \mathbf{A}\tilde{\mathbf{x}}_k + \mathbf{B}_{1d}\tilde{\zeta}_k + \mathbf{B}_{2d}\tilde{a}_k, \qquad \tilde{\mathbf{x}}_k \in \mathbb{R}^{n_{aug}},$$

$$\tilde{e}_k = \mathbf{C}_{1d}\tilde{\mathbf{x}}_k + D_d\tilde{a}_k, \qquad \tilde{e}_k \in \mathbb{R}^{p_e},$$

$$\tilde{y}_k = \mathbf{C}_{2d}\tilde{\mathbf{x}}_k + D_\theta\tilde{\theta}_{nk}, \qquad \tilde{\zeta}_k \in \mathbb{R}^{m_\zeta}, \tag{9}$$

where $\tilde{\zeta}_k$ is a unit variance, white-noise sequence and $n_{aug} = n_m + n_a + 4q$. The discrete-time cost functional is

$$V_d = \lim_{N\to\infty} \frac{1}{N} \sum_{k=0}^{N} \mathcal{E}\{\tilde{e}_k^T \tilde{e}_k\}. \tag{10}$$

The state vector in Eq. (9) can be partitioned as

$$\tilde{\mathbf{x}}^T = [\tilde{x}_m^T \quad \tilde{x}_{m2}^T \quad \tilde{x}_{m1}^T | \tilde{x}_a^T \quad \tilde{x}_{a2}^T \quad \tilde{x}_{a1}^T],$$

$$\tilde{x}_m \in \mathbb{R}^{n_m}; \tilde{x}_a \in \mathbb{R}^{n_a}; \tilde{x}_{m1}, \tilde{x}_{m2}, \tilde{x}_{a1}, \tilde{x}_{a2} \in \mathbb{R}^q. \tag{11}$$

The matrices that define discrete-time system (9) can be partitioned to conform with the state:

$$\mathbf{A} = \left[\begin{array}{cc} A_{dm} & 0 \\ 0 & \mathbf{A}_{da} \end{array}\right] = \left[\begin{array}{cccccc} A_{md} & 0 & 0 & 0 & 0 & 0 \\ A_{m1} & 0 & 0 & 0 & 0 & 0 \\ A_{m2} & I & 0 & 0 & 0 & 0 \\ 0 & 0 & 0 & A_{ad} & 0 & 0 \\ 0 & 0 & 0 & A_{a1} & 0 & 0 \\ 0 & 0 & 0 & A_{a2} & I & 0 \end{array}\right]. \tag{12}$$

$$\mathbf{B}_{1d} = \left[\begin{array}{c} 0 \\ \mathbf{B}_{a1d} \end{array}\right] = \left[\begin{array}{c} 0 \\ 0 \\ 0 \\ B_{ad} \\ B_{11} \\ B_{12} \end{array}\right], \qquad \mathbf{B}_{2d} = \left[\begin{array}{c} \mathbf{B}_{m2d} \\ 0 \end{array}\right] = \left[\begin{array}{c} B_{md} \\ B_{21} \\ B_{22} \\ 0 \\ 0 \\ 0 \end{array}\right], \tag{13}$$

$$\mathbf{C}_{1d} = [C_{m1d} \quad 0 \quad 0 | C_{a1d} \quad 0 \quad 0],$$

$$\mathbf{C}_{2d} = [0 \quad 0 \quad -(1/T_f)H | 0 \quad 0 \quad (1/T_f)H]. \tag{14}$$

The performance of AO system (8) is given in terms of cost functional of discrete-time system (10):

$$V = \frac{1}{T_f}(V_0 + V_d), \tag{15}$$

where V_d is given by Eq. (10) and

$$V_0 = \mathrm{tr}\left\{ C_a \int_0^{T_f} \int_0^{\sigma} e^{A_a \gamma} B_a B_a^T e^{A_a^T \gamma} \mathrm{d}\gamma \mathrm{d}\sigma C_a^T \right\}. \quad (16)$$

Thus, the continuous-time performance of the AO system can be determined directly from the performance of discrete-time system (9)–(14). The contribution V_0 is completely determined by the IWF model. Since this term is not affected by the controller, discrete-time system (9) can be used as a basis for controller design for the AO system.

3. OPTIMAL CONTROLLER

A. General LQG Solution

Selecting the controller to minimize discrete-time quadratic cost (10) will also minimize continuous-time performance (8) and hence maximize the Strehl ratio of the science signal (if the extended Maréchal approximation is valid [1,2]). The minimizing controller is given by the LQG solution if the exogenous noise sources $\tilde{\zeta}$ and $\tilde{\theta}_n$ are assumed to be Gaussian, or if the noises are assumed to be non-Gaussian but the controller is constrained to be LTI.

Regularization [14,16] has been used in LQG/H_2 problems to reduce the control amplitudes. The controller is chosen to optimally balance the residual variance and control effort. To allow the hybrid LQG solution to include regularization, quadratic penalties on the control signal will be incorporated into the hybrid LQG cost:

$$V_a = \lim_{W\to\infty} \frac{1}{N} \sum_{k=0}^{N} \mathcal{E}\{\tilde{a}_k^T D_a^T D_a \tilde{a}_k\},$$

$$V = V_d + V_a. \quad (17)$$

The hybrid LQG controller minimizes the cost V in Eq. (17) and is defined by the solutions of two AREs. The AREs use the quadratic cost and noise power spectral density (PSD) matrices:

$$\mathbf{Q} = \mathbf{C}_{1d}^T \mathbf{C}_{1d}, \qquad \mathbf{Q}_{xu} = \mathbf{C}_{1d}^T D_d, \qquad \mathbf{R} = D_d^T D_d + D_a^T D_a,$$

$$\mathbf{\Xi} = \mathbf{B}_{1d} \mathbf{B}_{1d}^T, \qquad \mathbf{\Theta} = D_\theta D_\theta^T. \quad (18)$$

The minimizing (LQG) controller is

$$\hat{\mathbf{x}}_{k+1} = (\mathbf{A} - \mathbf{L}\mathbf{C}_{2d})\hat{\mathbf{x}}_k + \mathbf{B}_{2d}\tilde{a}_k + \mathbf{L}\tilde{y}_k,$$

$$\tilde{a}_k = \mathbf{K}(\hat{\mathbf{x}}_k + \mathbf{L}_f(\tilde{y}_k - \mathbf{C}_{2d}\hat{\mathbf{x}}_k)). \quad (19)$$

The controller states $\hat{\mathbf{x}}_k$ are the estimates of states of discrete-time model (9) using measurements through sample $k-1$.

A symmetric, stabilizing, positive semidefinite solution to the control ARE exists if system (9)–(14) is stabilizable by $\mathbf{B}_{2d}$ and reconstructible from $\mathbf{C}_{1d}$ [21]. Since the DM and IWF models are stable, these conditions will be satisfied. The feedback gain $\mathbf{K}$ is obtained from the cost matrix $\mathbf{S}$:

$$\mathbf{S} = \mathbf{A}^T\mathbf{S}\mathbf{A} + \mathbf{Q} - (\mathbf{A}\mathbf{S}\mathbf{B}_{2d} + \mathbf{Q}_{xu})(\mathbf{B}_{2d}^T\mathbf{S}\mathbf{B}_{2d} + \mathbf{R})^{-1} \times (\mathbf{A}\mathbf{S}\mathbf{B}_{2d} + \mathbf{Q}_{xu})^T,$$

$$\mathbf{K} = -(\mathbf{B}_{2d}^T\mathbf{S}\mathbf{B}_{2d} + \mathbf{R})^{-1}(\mathbf{B}_{2d}^T\mathbf{S}\mathbf{A}^T + \mathbf{Q}_{xu}^T). \quad (20)$$

A symmetric, stabilizing, positive semidefinite solution $\mathbf{\Sigma}$ to the estimation ARE exists if system (9)–(14) is stabilizable by $\mathbf{B}_{1d}$ and reconstructible from $\mathbf{C}_{2d}$ [21]. Again, because the DM and IWF models are stable, these conditions will be satisfied. The estimation and innovations gains are obtained from the one-step prediction error covariance matrix $\mathbf{\Sigma}$:

$$\mathbf{\Sigma} = \mathbf{A}\mathbf{\Sigma}\mathbf{A}^T + \mathbf{\Xi} - \mathbf{A}\mathbf{\Sigma}\mathbf{C}_2^T(\mathbf{C}_2\mathbf{\Sigma}\mathbf{C}_2^T + \mathbf{\Theta})^{-1}\mathbf{C}_2\mathbf{\Sigma}\mathbf{A}^T,$$

$$\mathbf{L}_f = \mathbf{\Sigma}\mathbf{C}_2^T(\mathbf{C}_2\mathbf{\Sigma}\mathbf{C}_2^T + \mathbf{\Theta})^{-1}, \qquad \mathbf{L} = \mathbf{A}\mathbf{L}_f. \quad (21)$$

The discrete-time equivalent closed-loop AO system with controller (19) is stable [19,20]. In addition, the closed-loop hybrid AO system with controller (19) is stable [22].

B. Dimension Reduction for the Riccati Equations

Each of the AREs used to compute the gains for hybrid LQG controller (20) and (21) are $n_{aug} \times n_{aug}$ matrix equations. However, since many states are either unobservable through the cost J_d or uncontrollable by the process noise $\tilde{\zeta}$, the dimensions of the two AREs can be reduced.

The structure of performance output matrix $\mathbf{C}_{1d}$ (14) and system matrix (12) implies that the unobservable subspace of the performance variable contains the span of $\mathbf{x}_{\bar{o}}$:

$$\mathbf{x}_{\bar{o}}^T = [0 \quad \tilde{x}_{m2}^T \quad \tilde{x}_{m1}^T | 0 \quad \tilde{x}_{a2}^T \quad \tilde{x}_{a1}^T],$$

$$\tilde{x}_{m1}, \tilde{x}_{m2}, \tilde{x}_{a1}, \tilde{x}_{a2} \in \mathbb{R}^q. \quad (22)$$

Partition the cost matrix from Eq. (20) to conform with state partitioning (11) $\{\mathbf{S}=[S_{ij}]: i=1,\ldots,6; j=1,\ldots 6\}$. The cost submatrices associated with unobservable subspace are zero. Thus, $\{S_{ij}=0: i=2,3,5,6; j=2,3,5,6\}$.

Define the control ARE system, input, state, coupling, and cost matrices as

$$\mathbf{A}_c = \begin{bmatrix} A_m & 0 \\ 0 & A_a \end{bmatrix}, \qquad \mathbf{B}_c = \begin{bmatrix} B_{md} \\ 0 \end{bmatrix}, \qquad \mathbf{S}_c = \begin{bmatrix} S_{11} & S_{14} \\ S_{14}^T & S_{44} \end{bmatrix},$$

$$\mathbf{Q}_{xuc} = \begin{bmatrix} C_{m1d}^T D_d \\ C_{a1d}^T D_d \end{bmatrix}, \qquad \mathbf{R} = D_d^T D_d + R_a,$$

$$\mathbf{Q}_c = \begin{bmatrix} C_{m1d}^T C_{m1d} & C_{m1d}^T C_{a1d} \\ C_{a1d}^T C_{m1d} & C_{a1d}^T C_{a1d} \end{bmatrix}. \quad (23)$$

Then, control ARE (20) becomes

$$\mathbf{S}_c = \mathbf{A}_c^T\mathbf{S}_c\mathbf{A}_c + \mathbf{Q}_c - (\mathbf{A}_c\mathbf{S}_c\mathbf{B}_c + \mathbf{Q}_{xuc})(\mathbf{B}_c^T\mathbf{S}\mathbf{B}_c + \mathbf{R})^{-1}(\mathbf{A}_c\mathbf{S}_c\mathbf{B}_c + \mathbf{Q}_{xuc})^T. \quad (24)$$

The control gain (20) is

$$K_1 = (B_{md}^T S_{11} B_{md} + \mathbf{R})^{-1}(A_{md} S_{11} B_{md} + C_{m1d}^T D_d)^T,$$

$$K_4 = (B_{md}^T S_{11} B_{md} + \mathbf{R})^{-1}(A_{ad} S_{14}^T B_{md} + C_{a1d}^T D_d)^T,$$

$$\mathbf{K} = [\underbrace{K_1 \quad 0 \quad 0}_{\mathbf{K}_m} | \underbrace{K_4 \quad 0 \quad 0}_{\mathbf{K}_a}]. \tag{25}$$

Only the states associated with the discrete-time atmospheric model are controllable from the process noise. The noise-controllable space is contained in the span of $\mathbf{x}_u$:

$$\mathbf{x}_u^T = [0 \quad 0 \quad 0 | \tilde{x}_a^T \quad \tilde{x}_{a2}^T \quad \tilde{x}_{a1}^T],$$

$$\tilde{x}_a \in \mathbb{R}^{n_a}; \tilde{x}_{a1}, \tilde{x}_{a2} \in \mathbb{R}^p. \tag{26}$$

Partition the covariance matrix from Eq. (21) to conform with state partitioning (11) $\{\mathbf{\Sigma} = [\Sigma_{ij}] : i = 1, \ldots, 6; j = 1, \ldots 6\}$. The only nonzero blocks of $\mathbf{\Sigma}$ are $\{\Sigma_{1i} : i = 4, 5, 6; j = 4, 5, 6\}$.

Define the filter ARE system, output, noise, and covariance matrices as

$$\mathbf{C}_a = [0 \quad 0 \quad -(1/T_f)H], \qquad \mathbf{\Xi}_a = \mathbf{B}_{ad1}\mathbf{B}_{ad1}^T,$$

$$\mathbf{\Sigma}_a = \begin{bmatrix} \Sigma_{44} & \Sigma_{45} & \Sigma_{46} \\ \Sigma_{45}^T & \Sigma_{55} & \Sigma_{56} \\ \Sigma_{46}^T & \Sigma_{56}^T & \Sigma_{66} \end{bmatrix}. \tag{27}$$

Then the filter ARE becomes

$$\mathbf{\Sigma}_a = \mathbf{A}_{da}\mathbf{\Sigma}_a\mathbf{A}_{da}^T + \mathbf{\Xi}_a - \mathbf{A}_{da}\mathbf{\Sigma}_a\mathbf{C}_a^T(\mathbf{C}_a\mathbf{\Sigma}_a\mathbf{C}_a^T + \mathbf{\Theta})^{-1}\mathbf{C}_a\mathbf{\Sigma}_a\mathbf{A}_{da}^T. \tag{28}$$

The innovations and estimator gains are

$$\mathbf{L}_{fa} = \mathbf{\Sigma}_a\mathbf{C}_a^T(\mathbf{C}_a\mathbf{\Sigma}_a\mathbf{C}_a^T + \mathbf{\Theta})^{-1} \in \mathbb{R}^{(n_a+2p)\times p},$$

$$\mathbf{L}_f = \begin{bmatrix} 0 \\ \mathbf{L}_{fa} \end{bmatrix}, \qquad \mathbf{L} = \begin{bmatrix} 0 \\ \mathbf{A}_{da}\mathbf{L}_{fa} \end{bmatrix}. \tag{29}$$

Note that the quadratic cost matrices $\mathbf{Q}_c$, $\mathbf{Q}_{xu}$, and $D_d^T D_d$, and the process noise variance $\mathbf{\Xi}_a$ are available directly from the computation of the discrete-time model [3].

4. COMPARISONS WITH OTHER ADAPTIVE OPTICS CONTROLLERS

The hybrid LQG controller presented in Section 3 minimizes the residual wavefront variance for an AO system given models for each of AO system components (1)–(5). When the DM and IWF models are of a single (uncorrelated) mode of an AO system, the hybrid LQG controller is diagonal, where each diagonal element is single input, single output (SISO) (c.f. [5,7]). SISO models of the AO components can also be used (with a particular reconstructor [12]) when it can be assumed that the IWF and DM dynamics are uniform across the aperture.

Other control structures have also been used or proposed for use. These include modal gain-optimized integral controllers when the modal structure has been specified [4] and LQG controllers [10–16] based on a discrete-time model of the DM or IWF. This section will compare the performance of these controllers with the hybrid LQG controller. A major difference in the controllers is how the computational delay and continuous-time DM dynamics are handled. Insights into how these effects are handled by each of the designs can be clearly illustrated by SISO component models.

A. Incident Wavefront "Truth" Model

The AO system truth model is the model that is used as a basis for comparing the different control algorithm designs. To emphasize the effects of computational delays and DM dynamics, the truth model for this example will use SISO models for the AO system components with continuous-time, finite-dimensional models of the DM and IWF. The use of more detailed models to assess features such as multiple-input multiple-output (MIMO) performance or robustness with respect to modeling assumptions will be left for the future.

An atmospheric model that represents a good seeing night in Paranal, Chile, uses three layers with differing heights, Fried parameters, and wind speeds (see [23]). An effective height (5332 m), an effective Fried parameter ($r_0 = 0.17$ m at 500 nm), and an effective wind speed (17.7 m/s) were determined from the more detailed model. A von Karman model with an outer scale of 25 m, the effective height, and the effective Fried parameter were used to construct a single-phase screen to represent the atmosphere. These data were generated by taking samples of the wavefront at the center of the aperture every 0.00025 s when the phase screen was advanced across the aperture with the effective wind speed.

The IWF model approximates these data (see Fig. 2). The model is

$$G_m(s) = 1, \qquad G_a(s) = \frac{5000}{s+1}. \tag{30}$$

The WFS model is

$$H = 1, \qquad G_{WFS}(s) = \frac{1 - e^{-sT_f}}{sT_f}, \quad T_f = 0.001 \text{ s}. \tag{31}$$

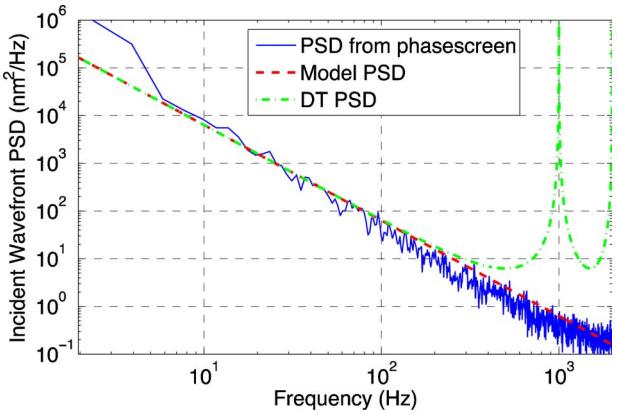

Fig. 2. (Color online) Solid curve is the estimated power spectrum of data obtained from a simulated von Karman phase screen that is representative of the Paranal Observatory site, Chile. The dashed line is the power spectral density (PSD) of the IWF model G_a. The dashed–doted curve is the PSD of a discrete-time (DT) IWF model used by the LQG controllers other than the hybrid LQG controller.

B. LQG Controllers Using a Discrete-Time Model

Several authors have investigated the use of LQG controllers based on discrete-time models of the components of an AO system [8–16]. Although individual models of the DM and WFS express the continuous-time dynamics of these devices, the models are converted to discrete time using various approximations. These approximations either ignore intraframe signal behavior (e.g., the IWF is assumed constant or linear over the frame) or only partially account for the loop dynamics (e.g., use of the step-invariant model for the DM and WFS).

Consequently, intraframe dynamics that can significantly affect performance are not incorporated into the models. The loss of performance caused by ignoring the intraframe variation of the IWF is small for short frame periods and typical atmospheric dynamics. However, the controller can cause significant performance degradation when the control application and measurement are asynchronous. Both effects will be illustrated here.

This subsection will compare three LQG controllers arising from different models: the hybrid LQG controller from this paper (hybrid LQG), the minimum variance controller from [12] (the discrete-time model LQG controller), and the LQG controller from [16] (the discrete-time IWF LQG controller). Each controller will be applied to a "truth" model consisting of a continuous-time DM model, ZOH, WFS, computational delay, and continuous-time IWF model (30) and (31). The corresponding hybrid model from [3] will be used to determine the residual root mean square (RMS).

The comparisons in Subsections 4.B and 4.C will use a "stiff" DM model (no temporal dynamics in continuous time) whose gain is normalized to unity

$$G_{DM}(s) = 1. \tag{32}$$

All controllers to be compared use discrete-time DM models derived from Eq. (32) that include the WFS and ZOH dynamics. The controller in [16] is valid only for synchronous operation between the WFS and ZOH—the control is not applied until the end of the next frame.

The sample values of IWF in [12] are modeled as a discrete-time random process. The measured (average) values of IWF in [16] are also modeled as a discrete-time random process. Because the controller in [16] is based a synchronous sampling, these two models are identical. To match the data PSD, the discrete-time IWF models for each controller will be $5/(z-0.999)$ (Fig. 2).

Figure 3(a) shows the residual variance [given by the hybrid model (9)–(14)] of AO systems with the three LQG controllers and no measurement noise as the computational loop delay varies from 0 to 2 frames. Figure 3(b) shows the same comparison but with a measurement noise whose standard deviation is $D_\theta = 200$ nm.

Note that the discrete-time IWF LQG controller is defined only for computational loop delays that are integer multiples of the frame period. For delays that are not integer multiples of the frame period, the commands generated by this controller are delayed until the next frame. When the delay is an integral number of frames, this discrete-time LQG controller and discrete-time IWF LQG controllers are identical.

The discrete-time LQG controller [12] performance exhibits performance degradation relative to that of the hybrid LQG controller both from not modeling the intraframe behavior of the IWF and from exciting intraframe errors with its control signal. For delays less than 1 frame, the dynamics of the DM and delay are modeled by the discrete-time transfer function ([9,12,15]):

$$G_m(z) = k_{DM}\frac{z-\alpha}{z^2}, \qquad \alpha = -\frac{\tau_c}{T_f - \tau_c}. \tag{33}$$

The zero of the discrete-time DM model moves from 0 (at $\tau_c = 0$) to $-\infty$ (at $\tau_c = T_f$) along the negative real axis. For delays less than a half-frame, the zero has a magnitude of less than 1 and is cancelled exactly by the discrete-time LQG controller. Due to this cancellation, the residual error is small at the times of output of the WFS (the frame times) even when the zero approaches $z = -1$ (half-frame delays). However, the intraframe residual can be arbitrarily large, leading to the residual variance spikes in Fig. 3. When the zero moves outside the unit circle, the corresponding discrete-time LQG controller pole (i.e., the pole that stably cancelled this zero when it was inside the unit circle) moves back toward the origin along the nega-

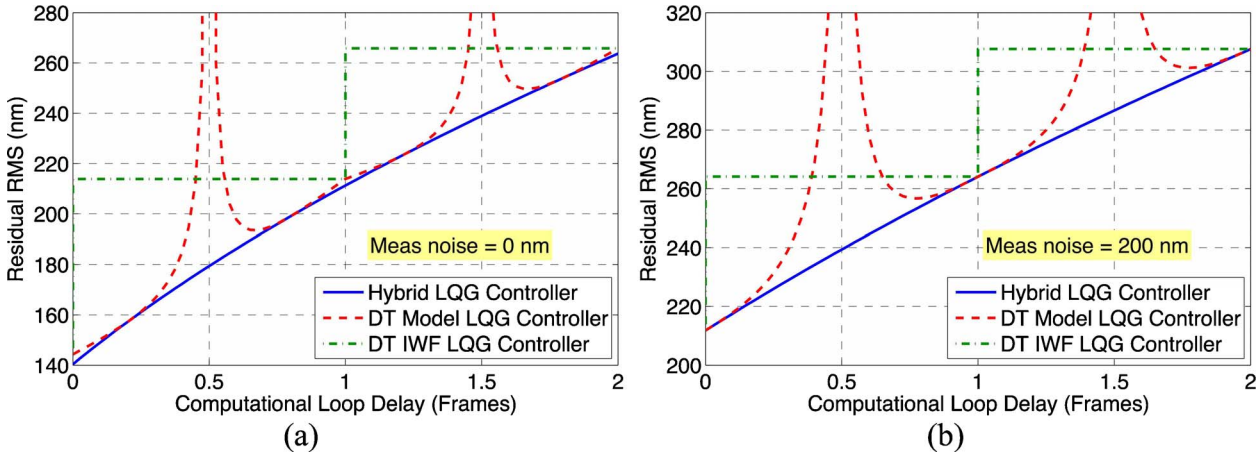

Fig. 3. (Color online) Residual RMS as a function of the computational loop delay for an AO system using LQG controllers based on different models: the hybrid LQG (solid curve), the discrete-time (DT) LQG controller (dashed curve), and the discrete-time IWF LQG controller (dashed–dotted curve).

tive axis, and the residual variance begins to decrease. This effect is amplified by the presence of measurement noise [compare Fig. 3(a) with Fig. 3(b)].

For delays greater than 1 frame, the transfer function in Eq. (33) is similar, with the computational delay τ_c replaced by $\bar{\tau}_c = \mathrm{mod}_{T_f} \tau_c$ and the denominator by $z^{\bar{n}+2}$, where $\bar{n} = \lfloor \tau_c / T_f \rfloor$. The same behavior—an increase in residual variance caused by the cancellation of the DM zero by the discrete-time LQG controller—occurs whenever the computational loop delay nears the middle of a frame.

Figure 3 also illustrates the penalty for using synchronous control architectures. By waiting to apply the commands until the next frame, the controller from [16] introduces an artificial computational delay that can result in an increase in the residual RMS. The increase is approximately 500 nm for computational loop delays that are only slightly greater than one frame period.

The effect of intraframe modeling of the IWF is seen for computational loop delays that are near-integer multiples of the frame period. The discrete-time models in [10,12,15,16] approximate the continuous-time IWF or its average by values sampled at the frame times. The degradation caused by this model becomes less as the frame period decreases. However, the degradation is noticeable in Fig. 3; Fig. 4 provides a zoomed-in view. For this frame rate (1 kHz) and IWF model (30), the degradation is about 1.2% (2.6 nm). For longer frame periods (such as used in retinal imaging) or more energetic wavefronts (such as in horizontal AO applications), the degradation caused by incorrect modeling of the intraframe IWF can be significant.

C. Comparison of LQG and Gain-Optimized Integral Controllers

The comparison of this section is based on a "truth" model that uses stiff DM model (32) and IWF model (30) shown in Fig. 2. The controllers will be assumed to be uniform over the entire aperture (or controllers for a single mode) and will be designed using an SISO model.

The most common AO control algorithm uses a discrete-time integrator with the gain optimized by mode (c.f. [1,2,4]). The transfer function of the integral controller is

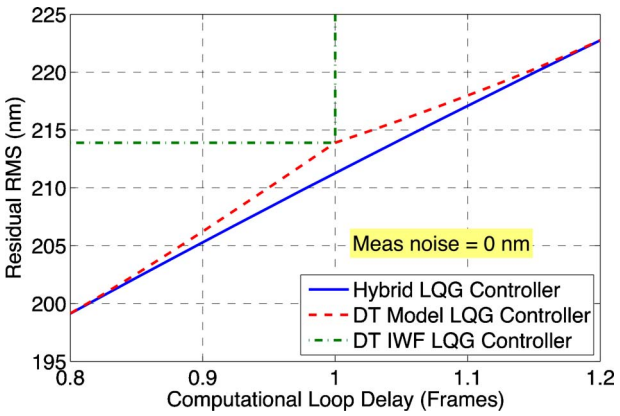

Fig. 4. (Color online) Zoomed view of the residual RMS of an AO system with the hybrid LQG controller (solid line), the discrete-time LQG controller (dashed curve), and the discrete-time IWF LQG controller (dashed–doted).

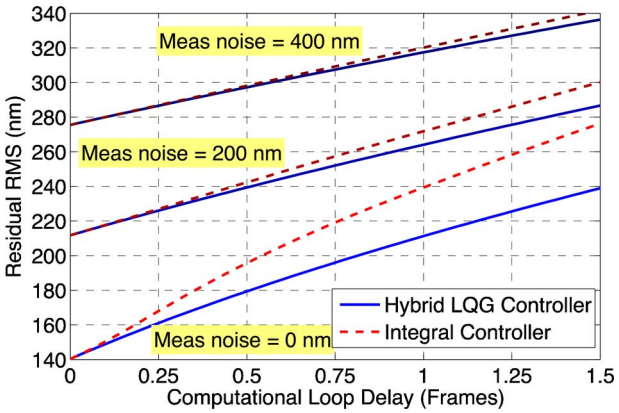

Fig. 5. (Color online) Residual RMS as a function of the computational loop delay for an AO system using the hybrid LQG controller (solid curve) and the gain-optimized integral controller (dashed curve). Three measurement noise levels are shown.

$$G_K(z) = \frac{K_I}{1 - z^{-1}}. \tag{34}$$

The gain K_I will be selected to minimize wavefront residual variance (8). The same gain is obtained by minimizing the variance V_d of the residual variable of the discrete-time model of the hybrid system with no regularization ($D_a = 0$). This optimization is performed using a golden search [24] for the parameter K_I with a tolerance of 10^{-6} nm^2.

Figure 5 shows the residual RMS produced by the hybrid LQG and gain-optimized integral controllers applied to the hybrid "truth" model for three measurement noise levels as a function of the computational loop delay. In each case, the residual RMS increases linearly with increasing loop delay. The increase in the residual RMS of the AO system with the integral controller is greater than that of the AO system with the hybrid LQG controller. For no measurement noise and a 1-frame sample delay, the relative increase is 13%.

The relative benefit of the hybrid LQG controller decreases as the measurement noise increases. For the highest measurement noise level shown in Fig. 5

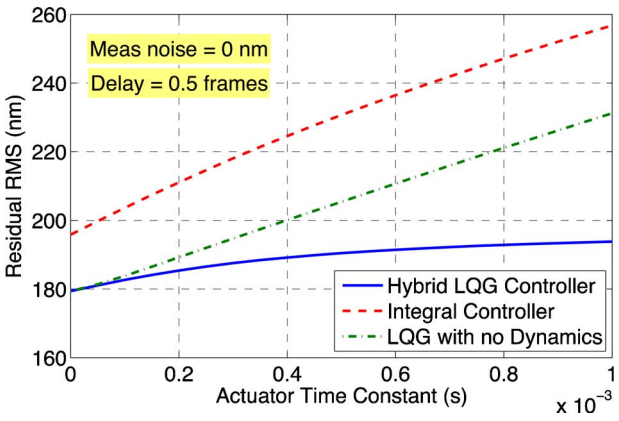

Fig. 6. (Color online) Residual RMS as a function of actuator time constant for an AO system using the hybrid LQG controller (solid curve), the gain-optimized integral controller (dashed curve), and the hybrid LQG controller designed using a stiff DM model (dashed–doted curve).

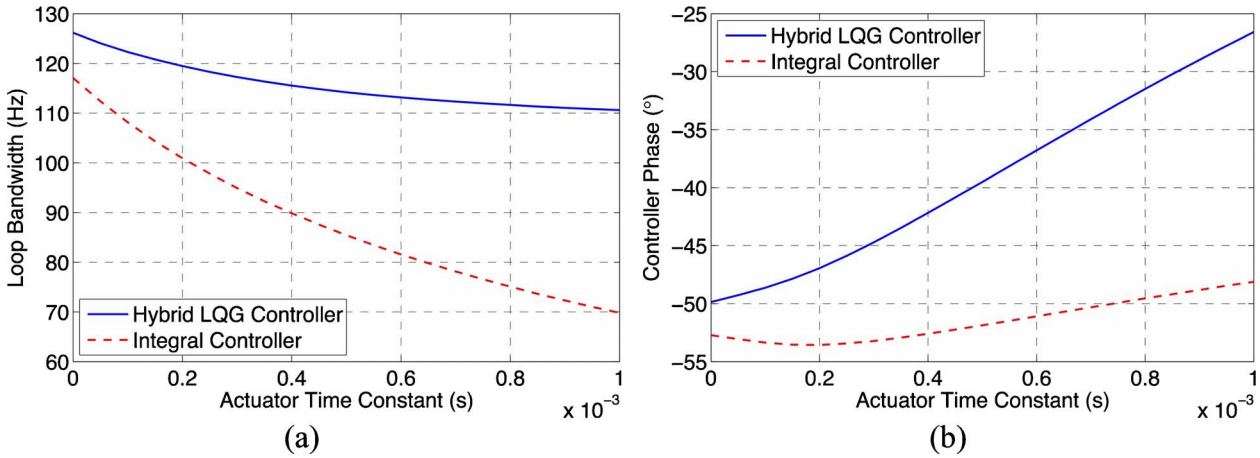

Fig. 7. (Color online) (a) Loop bandwidth and (b) controller phase at the loop bandwidth as a function of actuator time constant for an AO system using the hybrid LQG controller (solid curve) and the gain-optimized integral controller (dashed curve) x_2.

(400 nm) and a 1-frame delay, the improvement decreases to a little less than 1%. The hybrid LQG controller contains a lead filter that compensates for the loop delay. As the measurement noise level increases, the effect of the loop delay becomes dominated by the effect of the measurement noise.

D. Effect of Actuator Dynamics

The DM for this example will be modeled as having identical, first-order actuator lags with time constant τ_m, but with no structural dynamics. Since the actuator dynamics are uniform over the aperture, the controllers will be assumed to be uniform over the aperture (or controllers for a single mode) and will be designed using an SISO model. The continuous-time DM model is

$$\dot{x}_m(t) = -\frac{1}{\tau_m}x_m + \frac{1}{\tau_m}a(t),$$

$$s_m(t) = x_m(t). \tag{35}$$

Three controllers will be compared using the hybrid truth model constructed from the component DM model with actuator lag (35), IWF model (30), ZOH and WFS models (31), and a uniform computational loop delay of 0.5 frame. The first controller will be the hybrid LQG controller that uses dynamic DM model (35) to determine discrete-time design model (9)–(14). The second controller will be the gain-optimized integral controller defined in Subsection 4.C. This controller accounts for the effects of actuator dynamics by optimizing the integral gain as the controller lag increases. The third controller will be the hybrid LQG controller designed with stiff mirror model (30) but evaluated with dynamic DM model (35).

Figure 6 shows the resulting residual RMS for an AO system using these controllers as the actuator time constant increases. The hybrid LQG controller compensates for the increasing lag by providing increased temporal phase lead at the loop bandwidth while keeping the loop bandwidth nearly constant [see Fig. 7(a)]. The integral controller compensates for the actuator time constant by reducing the loop bandwidth significantly. The controller phase lead of the integral controller is fixed at any given frequency and increases only in Fig. 7(b) because of the reduced bandwidth.

5. CONCLUSION

The controller that minimizes the residual wavefront variance is a discrete-time LQG controller that can be computed from a hybrid model of the AO system. The LQG controller based on hybrid model (9)–(14) has several important features:

(1) The WFS and ZOH need not be synchronized.

(2) It can incorporate both DM and IWF dynamics. The hybrid LQG design can compensate for loop dynamics such as loop delays, DM dynamics, and vibrational modes (c.f., [10,13]).

(3) It is based on continuous-time models of both the DM and IWF. Consequently, the hybrid LQG design is based on an accurate representation of these dynamics, without increasing the complexity of the LQG design.

(4) It accounts for intrasample behavior of both the DM and the IWF. Thus, the hybrid LQG design avoids poor intersample control behavior that can plague other LQG designs. It also accounts for the intersample behavior of the IWF that can be significant in lower-frame-rate systems (such as in retinal imaging).

REFERENCES

1. J. W. Hardy, *Adaptive Optics for Astronomical Telescopes* (Oxford University Press, 1998).
2. M. C. Roggemann and B. M. Welsh, *Imaging through Turbulence* (CRC Press, 1996).
3. D. P. Looze, "Discrete-time model of an adaptive optics system," J. Opt. Soc. Am. A **24**, 2850–2863 (2007).
4. E. Gendron and P. Léna, "Astronomical adaptive optics. I: Modal control optimization," Astron. Astrophys. **291**, 337–347 (1994).
5. B. L. Ellerbroek, C. van Loan, N. P. Pitsianis, and R. J. Plemmons, "Optimizing closed-loop adaptive-optics performance with use of multiple control bandwidths," J. Opt. Soc. Am. A **11**, 2871–1886 (1994).

6. C. Dessenne, P.-Y. Madec, and G. Rousset, "Optimization of a predictive controller for closed-loop adaptive optics," Appl. Opt. **37**, 4623–4633 (1998).
7. L. A. Poyneer and J.-P. Véran, "Optimal modal Fourier-transform wavefront control," J. Opt. Soc. Am. A **22**, 1515–1526 (2005).
8. R. N. Paschall and D. J. Anderson, "Linear quadratic Gaussian control of a deformable mirror adaptive optics system with time-delayed measurements," Appl. Opt. **32**, 6347–6358 (1993).
9. D. P. Looze, M. Kasper, S. Hippler, O. Beker, and R. Weiss, "Optimal compensation and implementation for adaptive optics systems," Exp. Astron. **15**, 67–88 (2003).
10. B. Le Roux, J.-M. Conan, C. Kulcsár, H.-F. Raynaud, L. M. Mugnier, and T. Fusco, "Optimal control law for multiconjugate adaptive optics," J. Opt. Soc. Am. A **21**, 1261–1276 (2004).
11. D. M. Wiberg, C. E. Max, and D. T. Gavel, "A spatial non-dynamic LQG controller. Part II, theory," in *Procedings of 2004 IEEE Conference on Decision and Control* (IEEE, 2004), pp. 3333–3338.
12. D. P. Looze, "Minimum variance control structure for adaptive optics systems," J. Opt. Soc. Am. A **23**, 603–612 (2006).
13. C. Petit, J.-M. Conan, C. Kulcsár, H.-F. Raynaud, T. Fusco, J. Montri, and D. Rabaud, "First laboratory demonstration of closed-loop Kalman based optimal control for vibration filtering and simplified MCAO," Proc. SPIE, **6272**, 62721T-1–62721T-12 (2006).
14. C. Petit, J.-M. Conan, C. Kulcsár, H.-F. Raynaud, T. Fusco, J. Montri, and D. Rabaud, "Optimal control for multi-conjugate adaptive optics," C. R. Phys. **6**, 1059–1069 (2005).
15. K. Hinnen, M. Verhaegen, and N. Doelman, "Exploiting the spatiotemporal correlation in adaptive optics using data-driven H_2—optimal control," J. Opt. Soc. Am. A **24**, 1714–1725 (2007).
16. C. Kulcsár, H.-F. Raynaud, C. Petit, J.-M. Conan, and P. V. de Lesegno, "Optimal control, observers, and integrators in adaptive optics," Opt. Express **14**, 7464–7476 (2006).
17. H. S. Witsenhausen, "Separation of estimation and control for discrete time systems," Proc. IEEE **59**, 1557–1566 (1971).
18. E. I. Jury, *Sampled-Data Control Systems* (Wiley, 1958).
19. K. Ogata, *Discrete-Time Control Systems* (Prentice-Hall, 1987).
20. K. J. Åström and B. Wittenmark, *Computer-Controlled Systems* (Prentice-Hall, 1997).
21. P. Dorato and A. H. Levis, "Optimal linear regulators: the discrete-time case," IEEE Trans. Autom. Control **AC-16**, 613–620 (1971).
22. T. Chen and B. A. Francis, *Optimal Sampled-Data Control Systems* (Springer-Verlag, 1995).
23. R. Köhler, "CHEOPS performance simulations," MPIA Doc. no. CHEOPS-TRE-MPI-00033 (Max Planck Institüt fur Astronomie, 2004).
24. P. E. Gill, W. Murray, and M. H. Wright, *Practical Optimization* (Academic, 1981).